Mechanisms and Relative Rates of MX_2* Chemiluminescence in the Reactions of Ca, Sr, and Ba(^{1}S) Atoms with Dihalogen Molecules

P. Kierzkowski and A. Kowalski*

Institute of Experimental Physics, University of Gdansk, ul. Wita Stwosza 57, PL-80-952 Gdansk, Poland

D. Wren and M. Menzinger

Department of Chemistry, University of Toronto, Toronto, Ontario M5S 1A1, Canada

Received: April 18, 2000

Chemiluminescent reactions of ground state (Ca, Sr, and Ba) atoms with (Cl_2, Br_2, I_2, ICl, and IBr) were studied in a beam-gas arrangement. The MX_2* pseudo-continua were measured as a function of target gas pressure in the 0.0001−0.25 Pa range. To identify the main reaction channels that contribute to MX_2* formation and to obtain their relative contributions, kinetic models were fitted to the data. The following channels were considered: (1) radiative two-body recombination (R2BR), (2) radiative three-body recombination (R3BR), (3) two consecutive harpooning steps involving $MX^\dagger$ intermediate (two-step chemiluminescent reaction TSCR), and (4) combinations of the above. On their own, none of the mechanisms (1−3) provide satisfactory data fits. The best agreement is obtained by a model involving both R2BR and TSCR. The branching ratios of these channels were determined for $p = 0-0.25$ Pa. At 0.16 Pa these R2BR fractions vary from 7% (for Ca, Sr + ICl) to 79% (for Ba + IBr). Absolute CL cross sections and lower limits of photon yields were estimated by cross-calibrations. Photon yields for R2BR varied from 0.0004% to 0.037%, depending on the collision partners.

1. Introduction

The pseudo-continua arising from the $M(^1S_0) + X_2$ reactions of alkaline earth atoms with halogen molecules, first observed by Jonah and Zare,[1] are generally believed[1−18] to arise from metal dihalides MX_2*, whose electronic states remain a matter of speculation. The kinetics of emitter formation is interesting, complex, and controversial.

On the basis of the pressure dependence of the MX_2* spectrum, the pseudo-continuum was originally attributed to the *radiative two-body recombination* (R2BR) process:[1]

$$M(^1S_0) + X_2 \rightarrow MX_2^* \rightarrow MX_2 + h\nu \qquad (1)$$

If spectrally resolved at sufficiently low pressure, this emission would constitute a spectroscopy of the transition state.[19] More detailed studies[2−6,9] in the 0.1−5 mPa range showed that, in addition to a second-order process with a linear pressure dependence at the lowest pressures (called microTorr range; 1 Torr = 133 Pa), a quadratic, third-order process began to dominate in the mPa region (this can be clearly seen in Figure 2 of ref 6). Originally it was proposed[3,5,9] that this third order process involves the very fast collisional stabilization of a vibronically excited collision complex, followed by its radiative decay—a sequence called *radiative three-body recombination* (R3BR):

$$M + X_2 \leftrightarrow MX_2^{*\dagger} \qquad (2)$$

$$MX_2^{*\dagger} + X_2 \rightarrow MX_2^* + X_2 \qquad (3)$$

$$MX_2^* \rightarrow MX_2 + h\nu \qquad (4)$$

where the dagger denotes vibrational−rotational excitation. A rationalization of this mechanism requires extremely large stabilization cross sections $\sigma_s \geq 3000 \times 10^{-20}$ m^2 with a range of energy transfer $r_{ET} > 5 \times 10^{-9}$ m. Failing this, the complex lifetime would have to be unreasonably long ("immortal" complex). These facts stand against the R3BR mechanism.[15] However, R3BR was recently revived in the work of Gole et al.[12−14] to explain newly measured (purely quadratic in the 0.1−5 mPa range) pressure dependences of the chemiluminescence (CL) intensity and the appearance (or absence) of selected spectral features of MX_2* obtained under well-defined multiple collision conditions.

An alternative "pseudo-third-order" mechanism[3,5,9] involves two sequential harpooning steps,[15] also called a *two-step chemiluminescent reaction* (TSCR):

$$M + X_2 \rightarrow MX^\dagger + X \qquad (5)$$

$$MX^\dagger + X_2 \rightarrow MX_2^* + X \qquad (6)$$

$$MX_2^* \rightarrow MX_2 + h\nu \qquad (7)$$

In contrast to R3BR, where stabilization of the complex (3) must occur immediately after its formation (2), due to its short lifetime, in TSCR a long time may elapse before the $MX^\dagger$ radical

* Corresponding author: Institute of Experimental Physics, University of Gdansk, ul.Wita Stwosza 57, PL-80-952 Gdansk, Poland. Fax: (00-48)-(58)341-3175. E-mail: fizako@univ.gda.pl.

10.1021/jp001465e CCC: $19.00
Published on Web 08/12/2000

undergoes the second harpooning step (6). Furthermore, the ionization potential of vibrationally excited $MX^\dagger$ radicals is lower than that of M atoms. Hence the second harpooning step (6) is expected to be even faster than the first one. Both facts make the TSCR mechanism somewhat more plausible a priori than the competing R3BR mechanism.

The principal goal of the present work is therefore to settle the issue of competing reaction mechanisms in 15 reactions M + X_2, XY by a careful kinetic analysis of new detailed experiments.

The dependence of the MX_2* emission intensity I_{CL} on the number density n of target molecules is different for each of the three mechanisms considered above. For R2BR it is[1]

$$I_{CL}^{R2BR} \sim An \exp(-nx\sigma_M) \quad (8)$$

for R3BR it is[6,12]

$$I_{CL}^{R3BR} \sim Bn^2 \exp(-nx\sigma_M) \quad (9)$$

and for TSCR, in the experimental arrangement used, it is[11]

$$I_{CL}^{TSCR} \sim Cn[\exp(-nx\sigma_M) - \exp(-nx\sigma_{MX})] \quad (10)$$

To see clearly why the pressure dependence is linear, apart from the exponential attenuation terms, despite the fact that two target molecules are involved in the successive harpooning steps, (10) is rederived and discussed in the Appendix. In (8−10) *A*, *B*, and *C* are constants, *x* is the beam path length in the scattering cell, and σ_M and σ_{MX} are the total attenuation cross sections for the collisions of target gas molecules with M atoms and $MX^\dagger$ molecules, correspondingly.

We investigate here whether and to which extent these competing mechanisms contribute to the observed CL. We take a similar approach as that for (Ca, Sr) + I_2 reactions,[11] consider explicitly R3BR as a kinetic alternative, and apply the analysis to the 15 systems (Ca, Sr, Ba) + (Cl_2, Br_2, I_2, ICl, IBr). Measurements of the pressure dependence of pseudocontinua in the 0.0001−0.25 Pa range were least-squares fitted to (8−10) and to linear combinations of these expressions to provide an answer to this question. From the simulations, we derived the relative weights *A*, *B*, and *C* of the competing reaction paths as well as the attenuation cross sections σ_M for M atoms and σ_{MX} for $MX^\dagger$ radicals. We determined also the chemiluminescence cross sections σ_{CL} for the MX_2* emission, treated as if it was entirely due to a second-order process, by means of cross-calibration to the chemiluminescent reactions involving metastable alkaline earth atoms.[20,21] This is done under the assumption that the emitters radiate where they are formed (i.e., their radiative lifetime is $\tau_{rad} < 1\ \mu$s). Given the total collision cross sections and the CL cross sections, we then estimated the (pseudo-bimolecular) photon yields.

2. Experimental Section

The experimental setup is described elsewhere.[11] Briefly, the atomic beam effused from a resistively heated stainless steel oven. The temperature of the oven was $T = 1080$ K for Ca, $T = 1030$ K for Sr, and $T = 1130$ K for Ba, as measured with a chromel−alumel thermocouple. The scattering cell was heated to $T = 335$ K and was mounted above the beam source. One face of the cell had a quartz window which was covered by a mask with a slit (3 mm × 40 mm), fixing the beam path length in the gas at $x = (21 \pm 1.5)$ mm. The metals and halogens were supplied by Aldrich. The halogens, purified by repeated freeze−pump−melt cycles, were admitted to the scattering cell through an adjustable leak. Scattering pressures were in the range 0.0001−0.25 Pa, as measured with a capacitance manometer (MKS Baratron 120AD-00001RAU).

First the chemiluminescence spectra were recorded in the 300−900 nm range, using a 0.4 m Zeiss monochromator to establish the spectral regions in which the pseudo-continua are not overlapped by MX* emissions. The subsequent measurements of the MX_2* pressure dependence were made in the regions free of the MX* emission, using combinations of long wave and short wavelength cutoff filters or glass filters (Andover) and a bare Burle C31034 photomultiplier (cooled to $T = 250$ K), connected to a photon counting system. The target gas pressure was regulated with a Teflon needle valve, limiting flow from a back-up volume. It was always changed from high to low values.

The Mg*(^3P_J) + I_2 reaction was used to calibrate the chemiluminescence cross sections, since the Mg($^3P_1$−$^1S_0$) transition probability is known as internal clock, as critically discussed before.[22] The Mg* atoms were produced by passing the atomic beam through an electrical discharge. For a similar source, ca. 20% of alkaline earth atoms were in the metastable ^3P states[23]—the value used in the present work. The number density of the metal atoms was determined under the assumption that it is proportional to the number density in the oven;[24] i.e., it scales as (p_o/T_o). Since the oven temperature T_o was uncertain within ±10 K, the metal vapor pressure p_o obtained from the standard formulas[25] has a rather large error. This limits the accuracy of the absolute values of σ_{CL}. The resulting uncertainty of the CL cross sections does not exceed a factor of 2, when comparing the data for different metals. The uncertainty is much lower when comparing σ_{CL} values for the same metal M and different gases. The relative rates of light production in the M + (X_2, XY) reactions were thus compared in a single experimental run with a fixed M, and all target gases one after another. This procedure was repeated three time. Intensities agreed within 20%.

The absolute MX_2* chemiluminescence cross sections were determined by cross-calibration[20,21] with the known cross section for Mg* + I_2 → MgI(B′-X) reaction under identical kinetic conditions.

3. Results and Discussion

The CL pressure dependence was measured in the 0.0001−0.25 Pa range for 15 systems: (Ca, Sr, Ba) + (Cl_2, Br_2, I_2, ICl, IBr). For each system, three to eight experimental runs were made, each producing several hundred data points, which were collected by a computer. The values of adjustable parameters *A*, *B*, and *C*, and σ_M and σ_{MX}, in (8−10) were then obtained by least-squares fits. Figure 1 shows sample fits of the Ba + I_2 data to six models. Fitting attempts involving single reaction channels failed badly. R2BR alone (Figure 1a) cannot reproduce the nearly quadratic rise at low pressure and shows large deviations at higher pressures. The modeling with R3BR alone (Figure 1b) does not give the linear increase in the "microTorr regime" and fails throughout the pressure range covered, always deviating contrary to R2BR. TSCR does best, but the biggest problem with the simulation (Figure 1c) is that it does not give the observed linear increase of I_{CL} in the microTorr (<0.0005 Pa) region and in general reproduces poorly the experimental data in the low-pressure region (below 0.05 Pa).

Second, combinations of two mechanisms occurring simultaneously were probed (for Ba + I_2 − see Figure 1d−f). The data fits for R2BR + R3BR have three adjustable parameters

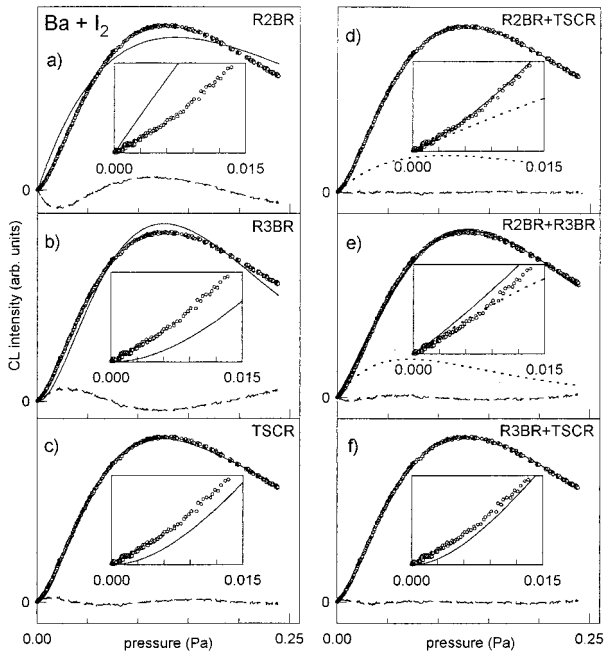

Figure 1. Best fits of the modeled chemiluminescence intensity (continuous lines) to the experimental data for Ba + I_2 (circles). Inserts show the low-pressure region. The fuzzy dashed lines (horizontal for R2BR+TSCR) correspond to the difference between the experimental points and the best fit. Dotted lines show partial contributions of R2BR to the MX_2* chemiluminescence intensity.

σ_M, *A*, and *B*. For R2BR+TSCR and R3BR+TSCR, four parameters are adjustable: σ_M, σ_{MX}, and *A*, *C* (or B, C). The quality of the fit is measured by the sum of squares of deviations (norm) Δ.

The results of the least-squares fits are collected in Tables 1−3. For each system, those experimental runs were retained which gave the values of σ_M and σ_{MX} that lie in the middle of the range of the values obtained from all runs (the maximal discrepancies were 15%). The values of σ_M and σ_{MX} obtained from these "average" runs are given in the third and fourth columns of Tables 1−3. In some cases (Sr + ICl, Sr + IBr, Ba + Cl_2, and Ba + ICl), the starting σ_M values were obtained from the attenuation of the MX* chemiluminescence; one can see that, in the course of fitting, the numbers were slightly readjusted, but remained close to the initial values, supporting the validity of the simulation procedure. For the other systems, the starting σ_M value was set about the same as for the most closely related reactive pairs. In general, the best fits are obtained for R2BR+TSCR, except for Ca + ICl, Ca + IBr, and Sr + ICl, where better fits were obtained for R3BR+TSCR.

The possibility of improving the R2BR+TSCR fits by adding a third component, R3BR, was not fully explored, but attempts in this direction gave results converging to the value $B \approx 0$, indicating that the addition of R3BR did not improve the fit. For the remaining part of this work it is important to note that a major fraction of the CL is due to R2BR.

It is interesting to compare the resulting σ_M and σ_{MX} values with calculated cross sections for the first and second harpooning steps of TSCR. The latter are collected in Table 4. For ICl and IBr targets only MCl and MBr are considered as the first-step products because of the substantially higher exoergicity of these exit channels. The highest possible vibrotational excitation energies $E(MX^{\dagger})$ are calculated from energy balance; it is further assumed that the ionization potential of MX product can be reduced by this value. The theoretical harpooning cross sections σ_{h1} are much smaller than the simulation parameters σ_M in Tables 1−3, probably because the latter reflect a substantial nonreactive scattering. However, the σ_{MX} and σ_{h2} values are often in good agreement, bearing in mind the large uncertainties of σ_{h2} due to accumulated errors of MX-ionization potentials and X_2,XY-electron affinities. For example, for Ca + ICl this uncertainty of σ_{h2} is (−50%; +100%). For Ca, Sr + ICl, and all Ba + X_2, XY, the second harpooning step leading to $MX^{+\dagger}$ + X_2^- (both ions in the ground state) produces some very large r_c and σ_{h2} which cannot be realized, since wave function overlap for the collision partners should be negligible at distances of $r_{c2} \geq 2$ nm and electron transfer or harpooning is highly unlikely over this distance. For these systems one has to consider the second harpooning step in the form $MX^{+\dagger} + X_2^-$*, where the halogen ion is in the excited electronic state. Little is known about the exact shape of the potential energy function for these excited states, but they are in general repulsive $^2\Pi$ states[31] with the same asymptote as for the ground-state X_2^-, so their excitation energy should be roughly equal to the X_2^- bond strengths. The latter are known for homonuclear X_2^- and are equal to 122, 111, and 100 kJ/mol for Cl_2^-, Br_2^-, and I_2^-, respectively;[32] for heteronuclear XY they can be calculated using thermochemical data[26] and are equal to 136 and 100 kJ/mol for ICl and IBr, respectively. The crossing radii r_c and second harpooning cross sections σ_{h2} calculated with the inclusion of electronic excitation of X_2^- to the lowest state are given in Table 4 in parentheses. The data are all reasonable for an efficient harpooning process.

TABLE 1: Attenuation Cross Sections σ_M and σ_{MX} (in 10^{-20} m^2) Obtained from Model Fits to Experimental Data and the Deviation Parameter Δ (arb. units)

system	model	σ_M[a]	σ_{MX}[a]	Δ[b]	remarks
Ca + Cl_2	R2BR + TSCR	114	512	1	good fit
	R2BR + R3BR	194		1.09	good fit
	R3BR + TSCR	137	1000	1.24	poor fit <0.03 Pa
	R2BR	84		2.33	poor fit throughout
	R3BR	257		3.53	very poor fit
	TSCR	101	1050	1.25	poor fit below 0.03 Pa
Ca + Br_2	R2BR + TSCR	175	615	1	good fit
	R2BR + R3BR	261		1.31	slight deviations throughout
	R3BR + TSCR	256	4017	1.18	good fit, but too high σ_{MX}
	R2BR	145		3.99	
	R3BR	339		7.65	
	TSCR	158	1394	2.23	poor fit below 0.05 Pa
Ca + I_2	R2BR + TSCR	184	650	1	very good fit
	R2BR + R3BR	289		3.85	poor fit throughout
	R3BR + TSCR	261	1296	1.73	poor fit below 0.04 Pa
	R2BR	142		15.52	
	R3BR	328		11.25	
	TSCR	174	840	2.79	poor fit below 0.04 Pa
Ca + ICl	R2BR + TSCR	194	371	1	good fit
	R2BR + R3BR	259		1.05	poor fit below 0.03 Pa
	R3BR + TSCR	254	1313	0.91	poor fit below 0.01 Pa
	R2BR	106		7.27	
	R3BR	273		1.85	slight deviations throughout
	TSCR	174	460	1.11	good fit
Ca + IBr	R2BR + TSCR	157	667	1	good fit
	R2BR + R3BR	255		1.85	
	R3BR + TSCR	230	1136	0.86	good fit
	R2BR	123		6.20	
	R3BR	299		5.12	
	TSCR	153	776	1.15	good fit

[a] Uncertainty ≤ 10%; [b] For each reactive system chosen as equal to 1 for R2BR + TSCR.

TABLE 2: Attenuation Cross Sections σ_M and σ_{MX} (in 10^{-20} m^2) from Model Fits to the Experimental Data, and Deviation Parameter Δ (arb. units)

system	model	σ_M[a]	σ_{MX}[a]	Δ[b]	remarks
$Sr + Cl_2$	R2BR + TSCR	208	315	1	good fit
	R2BR + R3BR	254		1.01	good fit
	R3BR + TSCR	254	1.2 ($\times 10^7$)	1.01	good fit; too high σ_{MX}
	R2BR	95		4.90	
	R3BR	276		2.03	
	TSCR	150	581	1.37	poor fit below 0.03 Pa
$Sr + Br_2$	R2BR + TSCR	185	691	1	slight deviation < 0.04 Pa
	R2BR + R3BR	296		2.74	poor fit
	R3BR + TSCR	270	1395	1.39	slight deviations throughout
	R2BR	139		11.88	
	R3BR	335		8.25	
	TSCR	176	887	1.92	poor fit below 0.1 Pa
$Sr + I_2$	R2BR + TSCR	191	687	1	very good fit
	R2BR + R3BR	291		3.26	
	R3BR + TSCR	267	1326	1.41	poor fit < 0.02 Pa
	R2BR	150		12.86	
	R3BR	332		9.89	
	TSCR	184	868	2.12	poor fit below 0.01 Pa
Sr + ICl	R2BR + TSCR	179	502	1	agrees with σ_M = 170 from SrCl*
	R2BR + R3BR	270		1.70	poor fit below 0.04 Pa
	R3BR+ TSCR	251	896	0.95	poor fit below 0.01 Pa
	R2BR	120		11.02	
	R3BR	291		3.97	
	TSCR	172	570	1.17	poor fit below 0.01 Pa
Sr + IBr	R2BR + TSCR	224	402	1	σ_M = 167 from SrBr*
	R2BR + R3BR	291		1.35	deviations <0.01 Pa, too high σ_M
	R3BR+ TSCR	292	6471	1.31	too high σ_M, σ_{MX}
	R2BR	120		23.10	
	R3BR	315		8.12	
	TSCR	184	634	4.38	

[a] Uncertainty ≤ 10%. [b] For each reactive system chosen as equal to 1 for R2BR + TSCR.

TABLE 3: Attenuation Cross Sections σ_M and σ_{MX} (in 10^{-20} m^2) Obtained from Model Fits to the Experimental Data and Standard Deviation Δ (arb. units)

system	model	σ_M[a]	σ_{MX}[a]	Δ[b]	remarks
$Ba + Cl_2$	R2BR + TSCR	196	761	1	σ_M = 195 from BaCl*(A+B)
	R2BR + R3BR	263		1.60	poor fit <0.1 Pa; too high σ_M
	R3BR + TSCR	268	1.7 ($\times 10^9$)	1.60	slight deviations; too high σ_{MX}
	R2BR	185		3.78	
	R3BR	382		19.82	
	TSCR	189	3194	3.23	very poor fit below 0.08 Pa
$Ba + Br_2$	R2BR + TSCR	202	636	1	very good fit
	R2BR + R3BR	202		2.48	poor fit above 0.04 Pa
	R3BR + TSCR	293	17280	2.81	poor fit >0.03 Pa; too high σ_{MX}
	R2BR	159		11.68	
	R3BR	405		26.50	
	TSCR	171	2627	8.74	
$Ba + I_2$	R2BR + TSCR	215	623	1	
	R2BR + R3BR	316		3.12	slight deviations throughout
	R3BR + TSCR	304	1890	2.12	poor fit <0.04 Pa; too high σ_{MX}
	R2BR	164		17.67	
	R3BR	358		12.82	
	TSCR	200	881	3.88	poor fit below 0.04 Pa
Ba + ICl	R2BR + TSCR	219	1687	1	σ_M = 199 from BaX*(A+B)
	R2BR + R3BR	282		2.80	poor fit <0.02 Pa; too high σ_M
	R3BR + TSCR	266	4214	1.80	poor fit <0.04 Pa; too high σ_{MX}
	R2BR	215		3.79	very poor fit below 0.03 Pa
	R3BR	402		21.21	
	TSCR	217	3491	2.14	very poor fit below 0.03 Pa
Ba + IBr	R2BR + TSCR	218	905	1	slight deviations below 0.005 Pa
	R2BR + R3BR	278		1.46	slight deviations below 0.01 Pa
	R3BR + TSCR	274	7249	1.34	poor fit <0.02 Pa; too high σ_{MX}
	R2BR	209		2.47	
	R3BR	412		17.05	
	TSCR	211	4741	2.08	

[a] Uncertainty ≤ 10%. [b] For each reactive system chosen as equal to 1 for R2BR + TSCR.

Table 5 contains the photon yields, calculated on the basis of R2BR. The second column gives the σ_M values from the best (R2BR+TSCR) fit. In the third column, the values of the absolute CL cross sections σ_{CL} are presented, calculated as if the MX_2* emission was due to a second-order process only. They were obtained by cross-calibration of the observed light intensity to that of the reference reaction $Mg^*(^3P_J) + I_2$. The σ_{CL} values for R2BR+TSCR in the third column were obtained at 0.16 Pa. They are lower limits since infrared emission is not accounted for. Note that the literature data cited in Table 5 for the pseudo-continuum were obtained at slightly different pressures.

Estimates of the MX_2* photon yields were obtained by dividing σ_{CL}(0.16 Pa), by the total collision cross sections σ_M. The results are shown in the fourth column of Table 5. The results are valid at the stated pressure and are lower limits. The percentage of R2BR or branching ratio, $\%^{R2BR}$(0.16 Pa), is given in the fifth column and was obtained as follows. After establishing the best fit *A*, *C*, σ_M, and σ_{MX} parameters from the (R2BR+TSCR) model, the parameter *C* was set to zero. The R2BR intensity was then obtained over the full 0−0.25 Pa range. The resulting truncated I_{CL}R2BR(p) values were then divided by the measured CL intensity, giving the percentage contribution of R2BR to the total intensity of the pseudo-continuum at each pressure. This contribution varies with pressure, since R2BR is a second order, and TSCR a "pseudo-third-order" process. An example of the pressure dependence of branching ratios is given in Figure 2 for $Ba + X_2$ reactions. From a pure R2BR spectrum at the lowest pressures, the emission evolves into a mixture of R2BR and TSCR emission. At 0.16 Pa (where all CL spectra were recorded) it gives the $\%^{R2BR}$ values in column 5. This percentage at 0.16 Pa, multiplied by the Φ_{CL}(0.16 Pa), gives a pressure independent value of Φ_{CL} for R2BR (in the last column of Table 5).

For M + ICl, IBr, one notes a correlation between the values of $\%^{R2BR}$ (fifth column) and the σ_{h2} values in the last column of Table 4. The latter are infinity for Ba + ICl, IBr, meaning that harpooning must occur to a vibronically excited BaX^{+}* + XY^- or $BaX^+ + XY^-$* state, with a considerably reduced cross section. Values of σ_{h2} calculated under the assumption that the lowest electronically excited XY^-* state is formed are given in parentheses. They agree much better with physical expectation.

TABLE 4: Ionization Potentials (IPs) of MX Molecules, IP(MX), Maximum Vibrational Excitation Energy of $MX^\dagger$ Produced in the $M + X_2$ Collision, $E(MX^\dagger)$, Ionization Energy of $MX^\dagger$, $IP(MX^\dagger)$ (All Values in kJ/mol), Curve Crossing Radii for the First and Second Harpooning Steps, r_{c1} and r_{c2}, (in 10^{-10} M) and Harpooning Cross Sections, σ_{h1} and σ_{h2} (in 10^{-20} m^2)

						$M + X_2$		$MX^\dagger + X_2$	
M	X_2	MX	IP(MX)[a]	$E(MX^\dagger)$[b]	$IP(MX^\dagger)$[c]	r_{c1}[d]	σ_{h1}[e]	r_{c2}[f]	σ_{h2}[g]
Ca	Cl_2	CaCl	541 ± 13	181	360	3.8	47	10.7	357
	Br_2	CaBr	534	173	361	4.0	51	12.1	460
	I_2	CaI	588	148	440	4.0	51	7.2	161
	ICl	CaCl	541 ± 13	213	328	4.4	61	25.7	2077
								(7.3)	(169)
	IBr	CaBr	534	195	339	4.0	51	15.0	707
Sr	Cl_2	SrCl	492 ± 6	179	313	4.3	59	16.7	881
	Br_2	SrBr	531	160	371	4.6	66	11.1	385
	I_2	SrI	531[h]	156	375	4.6	66	10.7	363
	ICl	SrCl	492 ± 6	212	280	5.0	80	240	2×10^5
								(9.8)	(300)
	IBr	SrBr	531	181	350	4.6	66	13.3	559
Ba	Cl_2	BaCl	483 ± 1	222	261	5.1	81	43.6	5982
								(9.1)	(261)
	Br_2	BaBr	482	229	253	5.9	108	206	1×10^5
								(11.8)	(438)
	I_2	BaI	482 ± 29	197	285	5.9	108	36	4072
								(10.0)	(314)
	ICl	BaCl	483 ± 1	256	227	6.6	139	∞	∞
								(15.7)	(771)
	IBr	BaBr	482	247	235	5.9	108	∞	∞
								(15.7)	(770)

[a] From ref 26 unless otherwise indicated. [b] Calculated from the reaction exoergicities. [c] Obtained by subtracting the values of $E(MX^\dagger)$ from the values of IP(MX); for ICl and IBr targets, the values given are for the more exoergic channels producing $MCl^\dagger$ and $MBr^\dagger$, correspondingly. [d] Curve crossing radius[27] $r_{c1} = e^2/(IP(M) - EA(X_2))$, ionization potentials of alkaline earth atoms:[28] IP(Ca) = 590 kJ/mol; IP(Sr) = 549 kJ/mol; IP(Ba) = 503 kJ/mol. Electron affinities of diatomic halogens:[28,29] $EA(Cl_2) = (230 \pm 10)$ kJ/mol, $EA(Br_2) = (246 \pm 10)$ kJ/mol, $EA(I_2) = (246 \pm 5)$ kJ/mol, EA(IBr) = (246 ± 10) kJ/mol, EA(ICl) = (274 ± 15) kJ/mol. [e] $\sigma_{h1} = \pi r_{c1}^2$. [f] $r_{c2} = e^2/(IP(MX^\dagger) - EA(X_2))$. The values in parentheses are for $EA(X_2)^*$, leading to formation of $X_2^- *$ in the lowest excited electronic state; see text. [g] $\sigma_{h1} = \pi r_{c1}^2$; see footnote f). [h] Reference 30.

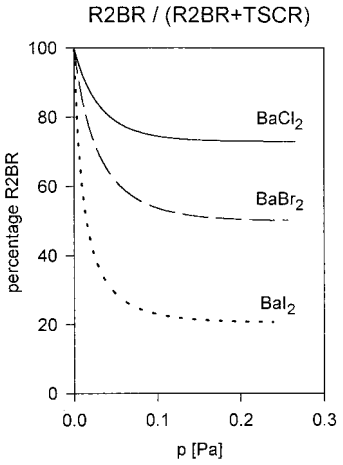

Figure 2. Pressure dependence of R2BR branching ratio for $Ba + X_2$ reactions from R2BR+TSCR model.

The MX_2^* spectra appear as pseudo-continua due to low resolution and spectral congestion. The emission contains probably A−X, B−X, and C−X transitions;[13] (there is only one theoretical paper considering potential energy surfaces for MX_2^*, concerning the $Ca + F_2$ system[33]). The shape of the CL pseudo-continua may vary with pressure because (1) the MX_2^* emissions caused by R2BR and TSCR may be different, (2) the percentage of R2BR varies with pressure, decreasing from ca. 99% for the lowest pressures to a plateau above 0.1 Pa. At the lowest pressures the CL spectrum from R2BR should dominate; with increasing pressure the R2BR signal will sometimes be outweighed by the TSCR signal. In our opinion, there were indications of such behavior in the previous studies.[12] In Table 4 of ref 12 relative $BaCl_2^*$ intensities recorded at 300 and 433 nm showed a substantial variation with pressure. Concerning the high percentage of R2BR for $Ba + Cl_2$, one can also note that the original claim,[1] that the $BaCl_2^*$ emission is purely R2BR, is almost true. The CL cross sections MX_2^* are biggest for Br_2 and I_2 targets. There is no obvious correlation between the trends in Table 5 and the experimental[12,34−37] and theoretical[38] structures of MX_2^*.

TABLE 5: Total Attenuation Cross Sections of Metal Atoms M, σ_M (in 10^{-20} m^2), Pseudo-Continuum Chemiluminescence Cross Sections per M Atom at Target Gas Pressure of 0.16 Pa, σ_{CL}(0.16 Pa) (in 10^{-20} m^2), Overall Photon Yields of the Pseudo-continuum at 0.16 Pa, Φ_{CL}(0.16 Pa) (in %), Percentage Contribution of R2BR to the Pseudo-continuum at 0.16 Pa, $\%^{R2BR}$(0.16 Pa), and Absolute Photon Yields of R2BR, Φ_{CL}^{R2BR} (in %)

system	σ_M[a]	σ_{CL} (0.16 Pa)	Φ_{CL} (0.16 Pa)[b]	$\%^{R2BR}$ (0.16 Pa)[c]	Φ_{CL}^{R2BR}[d]
$Ca + Cl_2$	114	0.016	0.014	42	0.006
$Ca + Br_2$	175	0.07	0.040	48	0.019
$Ca + I_2$	184	0.15	0.082	18	0.015
Ca + ICl	194	0.06	0.031	7	0.002
Ca + IBr	157	0.05	0.033	13	0.004
$Sr + Cl_2$	208	0.007	0.003	12	0.0004
$Sr + Br_2$	185	0.12	0.065	16	0.010
$Sr + I_2$	191	0.15	0.079	18	0.014
Sr + ICl	179	0.04	0.022	7	0.002
Sr + IBr	224	0.10	0.045	11	0.005
$Ba + Cl_2$	196	0.04[e]	0.020	73	0.015[f]
$Ba + Br_2$	202	0.15[g]	0.074	50	0.037
$Ba + I_2$	215	0.10[h]	0.047	21	0.010
Ba + ICl	219	0.017	0.008	59	0.005
Ba + IBr	218	0.05	0.023	79	0.018

[a] The values are obtained from the fitting procedure described in text; uncertainty ≤ 10%. [b] Calculated as $\sigma_{CL}(0.16\ Pa)/\sigma_M$. [c] Determined from computer fits. [d] Calculated as Φ_{CL}(0.16 Pa) times $\%^{R2BR}$(0.16 Pa), the Φ_{CL}^{R2BR} is independent of pressure. [e] Previous results: 0.3,[4] 0.1,[3] 0.0028,[9] 0.0011.[6] [f] Previous result: 0.0006.[6] [g] Previous result: 0.0013.[9] [h] Previous result: 0.0011.[9]

In conclusion, we obtained a direct experimental answer to the long-standing issue of the reaction channels contributing to MX_2^* formation. This was achieved, in the spirit of classical mechanistic kinetics, by fitting different plausible kinetic models to high quality pressure depencences. Accordingly, the sequence of two harpooning steps, TSCR, is the dominant third order process, and R3BR appears in fact to be at most a minor channel. This is in keeping with the estimated harpooning cross sections and the independence of the harpooning steps in TSCR, compared with the uncomfortably large complex stabilization cross section and long radiative lifetime of the collision complex required by the R3BR mechanism.

Acknowledgment. This work was supported within the research project KBN 2 P03 B 051 13.

Appendix

This section explains the difference in pressure dependence of chemiluminescence borne in R3BR and TSCR, both mechanisms requiring two collisions with X_2 molecules. Our considerations are valid for the experimental arrangement shown in Figure 3, where the atomic beam of number density $[M]_0$

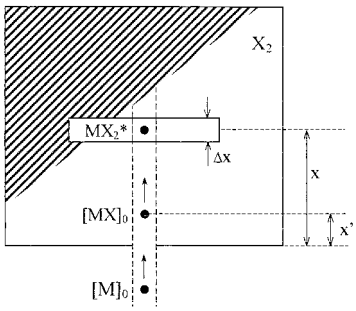

Figure 3. Schematic view of scattering cell and detection geometry.

enters the scattering cell filled with X_2 gas. As described in the Experimental section, a mask with a small slit of width Δx defines the scattering beam-path length x (a part of the mask is shown shaded in Figure 3). The MX_2* chemiluminescence is observed only through the slit. We assume that the radiative lifetime τ_R of MX_2* is short enough to give no loss of chemiluminescence due to escape of emitters from the observation window (from an effusive source the atomic beam comes with an average velocity on the order of 1 km/s; if MX_2* products are moving with similar velocity, then the condition is that τ_R does not exceed $\sim 1\ \mu$s). After the atomic beam enters the scattering cell, it is attenuated with cross section σ_M.

The derivation of the pressure dependence of MX_2* intensity for R3BR is straightforward. The phototube detects a signal when an M atom reaches the area seen through the slit and forms MX_2* by collision with an X_2 molecule while feeling the presence of another, stabilizing X_2 molecule. The chemiluminescence intensity I_{CL} for R3BR is

$$I_{CL}(MX_2^*) = Dk_{R3}n^2[M]_0 \exp(-nx\sigma_M) \qquad (A1)$$

where D is a detection (including geometry) factor, k_{R3} is the rate constant for R3BR, and n is the concentration of X_2.

The pressure dependence of MX_2* intensity for TSCR is quite different. An atom M, after travelling a distance x', collides with X_2 and the MX molecule is formed. This intermediate product can be scattered sideways; however, only the MX molecules scattered forward have a chance to contribute to the observed MX_2* chemiluminescence by colliding with an X_2 molecule at a location that can be viewed through the slit, i.e., at $x \pm 0.5(\Delta x)$. At x', the concentration of monohalide product is $[MX]_0$, the product is later attenuated with the total cross section σ_{MX} on its way $(x - x')$ to the observation window. MX can be formed anywhere between $x' = 0$ and $x' = x$. We integrate the contributions from all the places of origin of MX. Let us introduce two rate constants: k_{1h}, for the first harpooning step (forming MX), and k_{2h}, for the second, CL harpooning step forming MX_2*. One can write

$$I_{CL}(MX_2^*) = Dk_{2h}n[MX] \qquad (A2)$$

where [MX] is the concentration of MX in the observation window. Explicitly (A2) is

$$I_{CL}(MX_2^*) = Dk_{2h}' \cdot n \cdot \int_0^x [MX]_0 \exp[-n(x - x')\sigma_{MX}]\, dx' \qquad (A3)$$

where k_{2h}' is a "flux" rate constant (of dimension m^2/s, while k_{2h} has dimension of m^3/s), reflecting the fact that the MX substrate is collected from a tube of length x. The original concentration $[MX]_0$ can be unfolded, giving

$$\begin{aligned} I_{CL}(MX_2^*) &= Dk_{2h}'\, n\int_0^x k_{1h}n[M] \exp[-n(x - x')\sigma_{MX}]\, dx' \\ &= Dk_{1h}k_{2h}'[M]_0n^2 \times \int_0^x \exp(-nx'\sigma_M)\exp[-n(x - x')\sigma_{MX}]\, dx' \\ &= Dk_{1h}k_{2h}'[M]_0n^2 \exp(-nx\sigma_{MX}) \times \int_0^x \exp[-nx'(\sigma_M - \sigma_{MX})]\, dx' \\ &= Dk_{1h}k_{2h}'[M]_0n^2 \exp(-nx\sigma_{MX})n^{-1} \times (\sigma_{MX} - \sigma_M)^{-1}\{\exp[-nx(\sigma_M - \sigma_{MX})] - 1\} \\ &= (\text{constant})n[\exp(-nx\sigma_M) - \exp(-nx\sigma_{MX})] \end{aligned} \qquad (A4)$$

in agreement with (10). As σ_M is substantially smaller than σ_{MX} (see section 3), the first harpooning is the overall rate-determining step.

References and Notes

(1) Jonah, C. D.; Zare, R. N. *Chem. Phys. Lett*. **1971**, *9*, 65.
(2) Menzinger, M.; Wren, D. J. *Chem. Phys. Lett*. **1973**, *18*, 431.
(3) Wren, D. J.; Menzinger, M. *Chem. Phys. Lett*. **1973**, *20*, 471.
(4) Menzinger, M.; Wren, D. J. *Faraday Discuss. Chem. Soc*. **1973**, *55*, 312.
(5) Menzinger, M. *Chem. Phys*. **1974**, *5*, 350.
(6) D. J. Wren, D. J.; Menzinger, M. *Chem. Phys. Lett*. **1974**, *27*, 572.
(7) Dickson, C. R.; Kinney, J. B.; Zare, R. N. *Chem. Phys*. **1976**, *15*, 243.
(8) Mims, C. A.; Brophy, J. H. *J. Chem. Phys*. **1977**, *66*, 1378.
(9) Wren, D. J. Ph.D. Thesis, University of Toronto, 1978.
(10) Lu, R.; Li, F.; He, G.-Z.; Lou, N. *Chem. Phys. Lett*. **1986**, *131*, 339.
(11) Kierzkowski, P.; £awruszczuk, R.; Kowalski, A. *Chem. Phys*. **1995**, *190*, 131.
(12) Gole, J. L. *J. Chem. Phys*. **1995**, *102*, 7425.
(13) Gole, J. L.; Wang, H.; Joiner, J. S.; Dawson, D. E.; *J. Chem. Phys*. **1995**, *102*, 7437.
(14) Devore, T. C.; Gole, J. L. *Chem. Phys*. **1999**, *241*, 221.
(15) Menzinger, M. *Adv. Chem. Phys*. **1980**, *42*, 1.
(16) Menzinger, M. The M + X_2 Reactions: A Case Study. In *Gas Phase Chemiluminescence and Chemiionization*; A. Fontijn, A., Ed.; Elsevier Science Publishers: Amsterdam, 1985.
(17) Menzinger, M. *Acta Phys. Pol*. **1988**, *A73*, 85.
(18) Menzinger, M. The M + X2: Paradigms of Selectivity and Specificity in Electronic Multichannel Reactions. In *Selectivity in Chemical Reactions*: J. C. Whitehead, J. C., Ed.; Kluwer Academic Publishers: Amsterdam, 1988.
(19) Polanyi, J. C.; Zewail, A. H. *Acc. Chem. Res*. **1995**, *28*, 119.
(20) Dagdigian, P. J. *Chem. Phys. Lett*. **1978**, *55*, 239.
(21) Telle, H.; Brinkmann, U. *Mol. Phys*. **1980**, *39*, 361.
(22) Kowalski, A.; Menzinger, M. *Int. J. Mass Spectrom. Ion Processes* **1994**, *135*, 63.
(23) Brinkmann, U.; Steudel, A.; Walther, H. *Z. Angew. Phys*. **1967**, *22*, 223.
(24) Pauly, H. Other Low-Energy Beam Sources. In *Atomic and Molecular Beam Methods*; Scoles, G., Eds.; Oxford University Press: New York, 1988; Vol. 1, p 83.
(25) Landolt-Börnstein, *Zahlenwerte und Funktionen, 2a. Teil*; Springer: Berlin, 1960.
(26) Lias, S. G.; Bartmess, J. E.; Liebman, J. F.; Holmes, J. L.; Levin, R. D.; Mallard, W. G. *J. Phys. Chem. Ref. Data* **1988**, *17*, Suppl. 1.
(27) Levine, R. D.; Bernstein, R. B. *Molecular Reaction Dynamics and Chemical Reactivity*; Oxford University Press: New York, 1987.
(28) Weast, R. C., Ed. *CRC Handbook of Chemistry and Physics*, CRC Press: Boca Raton, 1985.

(29) Ross, U.; Schulze, Th.; Meyer, H. J. *Chem. Phys. Lett.* **1985**, *121*, 174.
(30) Kleinschmidt, P. D.; Hildenbrand, D. L. *J. Chem. Phys.* **1978**, *68*, 2819.
(31) Person, W. H. *J. Chem. Phys*. **1963**, *38*, 109.
(32) Huber, K. P.; Herzberg, G. *Molecular Spectra and Molecular Structure, Vol. 4. Constants of Diatomic Molecules*; Van Nostrand Reinhold: New York, 1979.
(33) Yarkony, D. R.; Hunt, W. J.; Schaefer, H. F., III *Mol. Phys*. **1973**, *26*, 941.
(34) Buchler, A.; Stauffer, J. L.; Klemperer, W.; Wharton, L. *J. Chem. Phys*. **1963**, *39*, 2299.
(35) Buchler, A.; Stauffer, J. L.; Klemperer, W. *J. Chem. Phys*. **1964**, *40*, 3471.
(36) Buchler, A.; Stauffer, J. L.; Klemperer, W. *J. Am. Chem. Soc*. **1964**, *86*, 4544.
(37) Wharton, I.; Berg, R. A.; Klemperer, W. *J. Chem. Phys*. **1966**, *39*, 2023.
(38) Seijo, L.; Barandiaran, Z.; Huzinaga, S. *J. Chem. Phys.* **1991**, *94*, 3762.